Drug Delivery Nanotubes

Deutsche Ausgabe: DOI: 10.1002/ange.201508710
Internationale Ausgabe: DOI: 10.1002/anie.201508710

# Visible-Light-Triggered Drug Release from $TiO_2$ Nanotube Arrays: A Controllable Antibacterial Platform

*Jingwen Xu, Xuemei Zhou, Zhida Gao, Yan-Yan Song,* and Patrik Schmuki**

***Abstract:*** *In this work, we use a double-layered stack of $TiO_2$ nanotubes (TiNTs) to construct a visible-light-triggered drug delivery system. The key for visible light drug release is a hydrophobic cap on the nanotubes containing Au nanoparticles (AuNPs). The AuNPs allow for a photocatalytic scission of the hydrophobic chain under visible light. To demonstrate this principle, we loaded ampicillin (AMP) into the lower part of the $TiO_2$ nanotube stack, triggered visible-light-induced release, and carried out antibacterial studies. The release from the platform becomes most controllable if the drug is silane-grafted in the hydrophilic bottom layer for drug storage. Thus, visible light photocatalysis can also determine the release kinetics of the active drug from the nanotube wall.*

Controllable drug delivery has attracted wide interest in biomedicine and other fields of science to achieve targeted use of an active substance at the right time and place. In particular, drug release mechanisms with triggers that respond to surrounding factors, such as pH,[1] temperature,[2] illumination, and ionic strength[3] are of high practical significance. Many nanomaterials are, or can be designed to be particularly sensitive to environmental factors. Biocompatible systems have been developed to improve the feasibility of targeted drug delivery with a much higher control over the pharmacokinetics (which can decrease systemic toxicity).[4–7]

A wide range of potential drug carries have been explored, including nanoparticles,[8] microgels,[9] nanotubes,[10,11] and polymeric micelles.[2b,12] Drug carriers based on nanotubes, in particular, have various beneficial features owing to their intrinsically high surface-to-volume ratio, well-defined geometry, and stable structure.[13] In the past decade, $TiO_2$ nanotube arrays (TiNTs) grown by a self-organizing electrochemical anodization process have attracted tremendous scientific interest owing to the combination of geometric features with inherent photocatalytic activity.[14] Furthermore, biocompatible scaffolds for hosting functional guest molecules can be fabricated, taking advantage of the large number of hydroxy groups present on the tube walls. These provide the possibility of incorporating desired functional groups, loading drugs, or grafting capping molecules and thereby establish advanced storage and release mechanisms by UV light irradiation.[15] However, UV light only accounts for 2–4% of solar energy, and as a result such a trigger mechanism will not respond robustly to solar light. Even more importantly, many biomolecules suffer from denaturation or decomposition when extensively exposed to UV light.

Herein, we introduce a visible-light-triggered drug delivery platform where the trigger for releasing the drug is based on gold surface-plasmon resonance (Au-SPR)-induced photocatalytic chain scission of a hydrophobic cap on the nanotubes. As an example, we demonstrate controllable antibacterial activity by releasing the antibiotic drug, amipicillin (AMP), under visible light.

Scheme 1 illustrates the steps used for the preparation of this TiNT-based platform. It consists of two parts: the top hydrophobic layer that acts as a cap, and the lower hydrophilic layer that serves for antibacterial drug storage. For synthesis (for details, see the Supporting Information, Figures S1–S3), first, a $TiO_2$ nanotube layer was grown in a glycerol/water/$NH_4F$ electrolyte to a thickness of approximately 0.3 μm, with individual nanotube diameters of 90 nm (Figure 1 A, B). The as-formed amorphous nanotubes were then crystallized to anatase by annealing at 450 °C in air for 1 h (anatase provides a much higher photocatalytic activity than amorphous material). AuNPs were decorated on the tube wall and entrance (Figure 1 C, D) by a biotemplated method that we reported previously (outlined in Figure S1).[16] After Au decoration, a hydrophobic monolayer of octadecylphosphonic acid (ODPA) was attached to the tube walls (the successful decoration of AuNPs and ODPA was characterized by XPS, as shown in Figure S3). The sample was subsequently anodized again in an ethylene glycol/$NH_4F$ electrolyte. In contrast to water-based electrolytes, ethylene glycol electrolytes enter into the hydrophobic tubes and thereby allow for a second anodic tube to grow through the bottom of the first tube layer. The voltages for second anodization were chosen to match the nanotube diameter in the first layer (30 V). The length of the lower layers is controlled by the duration of the second anodization. As shown in Figure 1 B, the side view verifies that nanotubes can grow aligned to the upper layer during the second anodization (the lengths of the second layer used were about 1.7 μm, determined by the 3 h duration of the second anodization).

After the growth of the lower layer, dodecanethiol (NDM) was used to coat the defects formed in the ODPA hydrophobic layer during the second anodization to strengthen the overall hydrophobic nature of the cap layer.

[*] J. Xu, Dr. Z. Gao, Prof. Dr. Y.-Y. Song
College of Sciences, Northeastern University
Shenyang 110004 (China)
E-mail: yysong@mail.neu.edu.cn
X. Zhou, Prof. Dr. P. Schmuki
Department of Materials Science, WW4-LKO
University of Erlangen-Nuremberg
Martensstrasse 7, 91058 Erlangen (Germany)
E-mail: schmuki@ww.uni-erlangen.de

Supporting information for this article is available on the WWW under http://dx.doi.org/10.1002/anie.201508710.

  

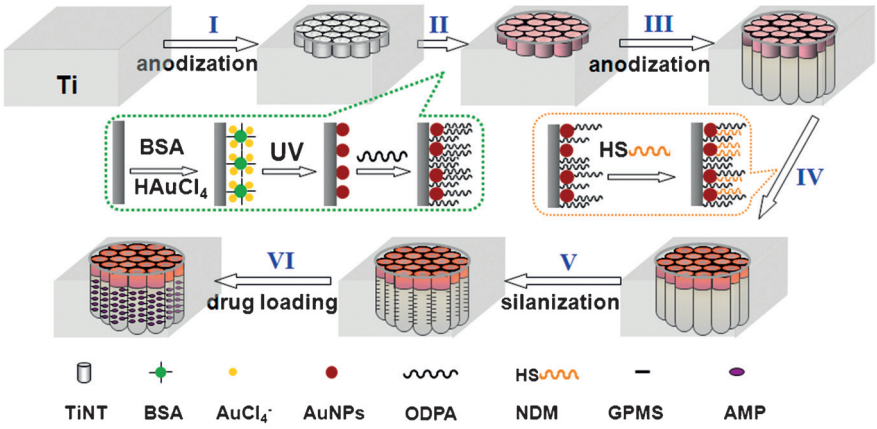


***Scheme 1.*** Preparation of visible-light-controlled drug-release TiNTs. I) First anodization to form TiNTs; II) Decoration of Au nanoparticles and hydrophobic monolayer to TiNTs; III) Second anodization to allow nanotube continue to grow for drug storage; IV) Link of hydrophobic monolayer to Au nanoparticles by mercaptan; V) Silanization of lower layer with GPMS; VI) AMP loaded by GPMS linker (details are shown the Supporting Information, Figure S2).

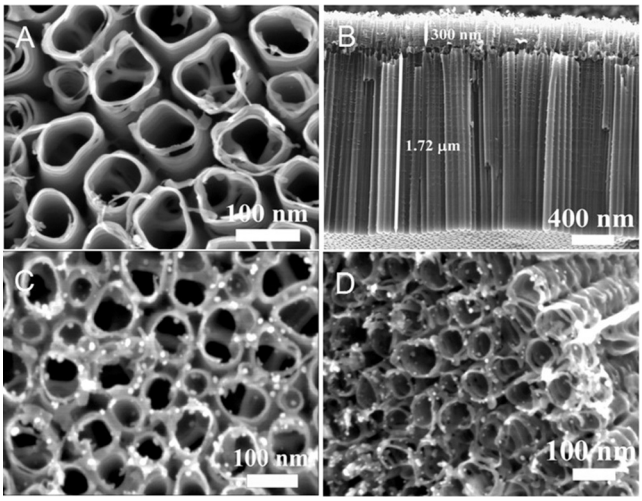


***Figure 1.*** SEM images of A) top-view images and B) cross-sectional images for double nanotube layers TiNTs; C) top-view and D) cross-sectional images for upper nanotube layers of TiNTs/AuNPs-ODPA.

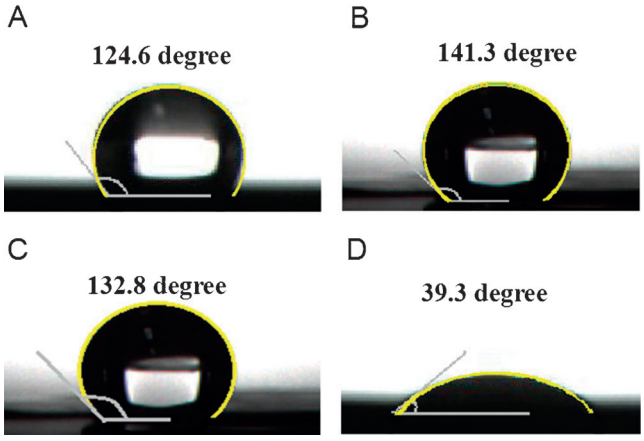


***Figure 2.*** Optical images of a water droplet on TiNTs/AuNPs: A) after modification with ODPA, B) after modification with thiole NDM, C) after loading with AMP, and D) after releasing AMP by visible light illumination for 30 min.

To load the lower part of the tubes with the AMP, (3-glycidyloxypropyl) trimethoxysilane (GPMS) molecules were first attached to the walls of the lower part of the nanotubes, and then the samples were immersed in an ethanol solution of AMP. AMP molecules react with the silane linker to form a covalent bond (outlined in Figure S2).[17] To characterize the effect of the different preparation steps on the surface wettability, we measured water droplet contact angles ($\theta\omega$) after critical synthesis steps (Figure 2). The annealed TiNTs and TiNTs/AuNPs show a completely hydrophilic wetting characteristic ($\theta\omega \approx 0$). After incubation with ODPA, which attaches to the wall of the nanotubes, the surface of the sample showed a strongly hydrophobic character with $\theta\omega =$ 124.6° (Figure 2 A). After the second anodization, the contact angle exhibited a slight decrease, but the hydrophobic outer nature was maintained with $\theta\omega =$ 104.2° (Figure S5). This demonstrated that most of the ODPA molecules in the first layer can withstand the second anodization step in the fluoride-containing ethylene glycol electrolyte. The second incubation in dodecanethiol (NDM), which decorates the Au nanoparticles, leads again to an increase in the contact angle to $\theta\omega = 141.3°$ (Figure 2 B). Only a slight decrease in the contact angle ($\theta\omega = 132.8°$) was observed after attachment of the silane and AMP to the walls of the lower nanotubes. This illustrated the strongly hydrophobic character of the tube layer surface after the entire synthesis of the drug-loaded platform. These processes were characterized by XPS (Figure S3).

To evaluate visible light activity introduced by the Au nanoparticle loading and successful electronic coupling of Au with the $TiO_2$ tubes, we acquired not only reflectivity data (Figure 3 A), but also photocurrent spectra (Figure 3 B). The light absorption data show an Au nanoparticle-induced absorption behavior in the visible range, peaking at approximately 526 nm (curve b, Figure 3 A) owing to SPR.[18,19] The photograph (inset of Figure 3 A) of the amphiphilic $TiO_2$ nanotube arrays after Au nanoparticle decoration also shows the pink color typical for the SPR of Au nanoparticles. The photocurrent spectra for the AuNP-containing sample show an redshifted onset and an enhancement (curve b, Figure 3 B) over the entire spectral range. This broad enhancement can be explained by: once visible light absorption takes place, photocatalytic decomposition of the organic monolayer can begin,[20] that is, once the first hydrophobic organic chains are broken, wetting of the tube tops increases,

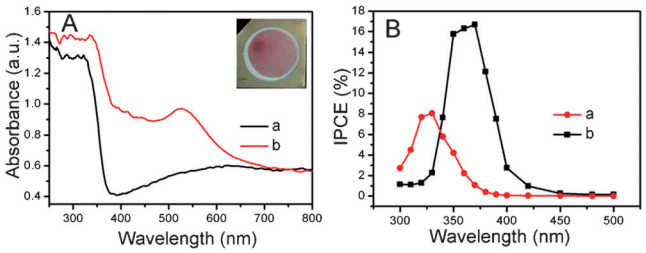


***Figure 3.*** A) UV/Visible diffuse reflectance spectra of anatase $TiO_2$ nanotube arrays (curve a) and the amphiphilic $TiO_2$ nanotube arrays decorated with Au nanoparticles (curve b). Inset: photograph of the amphiphilic $TiO_2$ nanotube arrays with Au nanoparticle decoration. B) Incident photon-to-current conversion efficiency (IPCE) of ODPA decorated TiNTs (curve a) and ODPA-decorated AuNPs/TiNTs (curve b)in an aqueous solution of 0.1 M $Na_2SO_4$ at an applied bias of +0.5 V versus saturated calomel electrode (SCE).

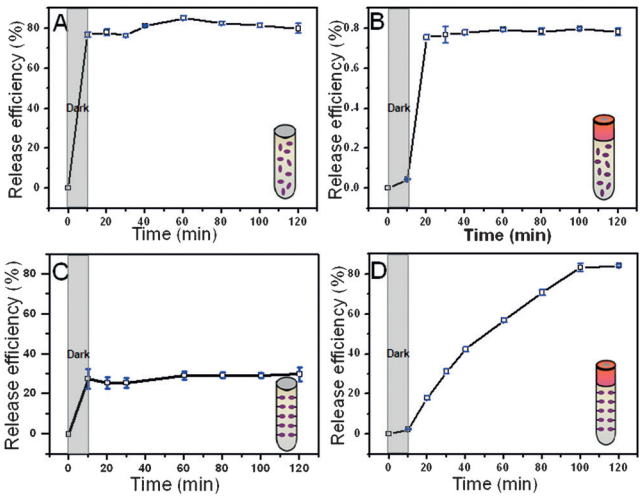


***Figure 4.*** Release efficiency of AMP from the nanotubes. Four methods for drug loading using AMP as a hydrophilic model drug: A) immersion without any $TiO_2$ surface modification; B) immersion after ODPA modification in the upper nanotube layer (hydrophobic cap); C) covalently attached HRP over the entire nanotube layers; and D) ODPA cap in the upper nanotube layer and covalently attached HRP in the lower nanotube layer.

providing better electrolyte access to the nanotube arrays, thereby enhancing charge transfer and the photocurrents.

To evaluate visible light activity under conditions without an applied bias (OCP), we carried out a color reaction test (Figure S6) to demonstrate the formation of $H_2O_2$. The positive reaction for gold-decorated tubes (and the negative results on a non-decorated reference) strongly support the hypothesis that Au-SPR can provide a conduction-band-induced photocatalytic pathway.[20a] The excitation and flow of electrons from the Au deposits to the conduction band (CB) of $TiO_2$ have been reported for such systems,[20b] but the decorated Au nanoparticles can also serve as trapping centers for electrons photogenerated in the CB of $TiO_2$. Under visible light conditions, this may lead to an improved photocatalytic efficiency for AuNP-decorated TiNTs, mainly by conduction-band-induced $O_2^{\bullet}$ and peroxide or $OH^{\bullet}$ formation.[20] Further experiments (Figure S7) identified the formation of $OH^{\bullet}$ by using an established fluorescence method based on terephthalic acid.[21] These active species can diffuse several micrometers[22] in the electrolyte, and thus also cut the linker in the lower part of the tubes. In the UV range, photo-induced valence band holes can further contribute and break hydrophobic chains by direct hole transfer or $OH^{\bullet}$ formation.[23]

To demonstrate that the present system indeed can show effective and controllable release of a real drug under bias-free and visible-light-only conditions, AMP release kinetics were studied for different drug-anchoring and -capping stages (Figure 4). For this, samples were exposed to a xenon light source (with a filter of $\lambda > 420$ nm, illumination intensity 50 mW cm$^{-2}$) after immersion into deionized water (5 mL), and kept in the dark for 10 min. To detect the released drug, we used UV/Vis spectrometry (after reaction with ninhydrin, Figure S8). As seen in Figure 4A, if AMP is loaded only by dipping (neither cap nor linker is used), a quick and uncontrolled release is obtained. Most of the drug molecules are released from the nanotubes within the first 10 min (that is, the dark period). With hydrophobic Au caps, AMP is retained within the tubes in the dark, but the drug molecules are released immediately after the removal of the upper cap by visible light (Figure 4B). Figure 4C shows the drug release kinetics for hydrophilic nanotubes, in which AMP is covalently linked with the tube wall by GPMS but no Au coating cap is present. In this case, there are almost no AMP molecules released under light owing to a lack of photocatalytic activity. This demonstrates that visible light cannot trigger the release of AMP without grafting AuNPs on the tubes. Figure 4D shows the results from amphiphilic TiNTs where AuNPs were introduced into the hydrophobic cap and AMP is covalently linked to the lower tube walls. These layers enable an illumination-controlled release. In the first dark period, there is a very minor release that can be ascribed to small amount of physical adsorbed AMP still present. Upon illumination, however, hydrophobic ODPA molecules on the first nanotube layer are decomposed, the GMPS linkers are cut, and AMP molecules are controllably released.

To confirm full functionality of this platform, we investigated the release of AMP in a bacterial culture test. *Escherichia coli*, which is responsible for many infections in daily life, served as a model target microorganism for antibacterial tests. In Figure 5A, the antibacterial activity from hydrophilic TiNTs (anatase tube without AMP-loading) and empty amphiphilic AuNPs/TiNTs (without AMP-loading) were compared with the amphiphilic AuNPs/TiNTs loaded with AMP. The amphiphilic nanotubes loaded with AMP showed an effective bactericidal activity under visible light irradiation.

The hydrophilic nanotubes and the empty amphiphilic AuNPs/TiNTs exhibit only weak bactericidal activity. We further evaluated the controllability of the drug delivery system by releasing the drug after different illumination periods (Figure 5B). The results indicate a light-controllable amount of drug was released, corresponding to the illumination duration. In these experiments the bactericidal effect tapers off after 90 min, suggesting that at this point most of the available drug molecules are released. The influence of

  

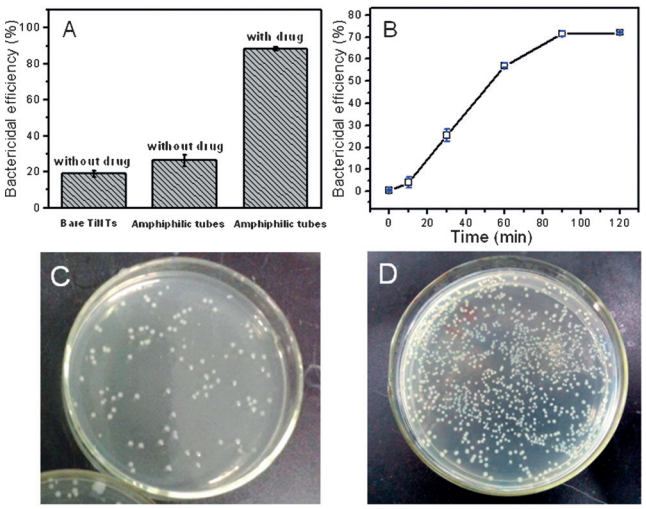


***Figure 5.*** The bactericidal efficiency of A) bare TiNTs, and amphiphilic TiNTs with and without drug loaded under visible light irradiation. B) AMP-loaded amphiphilic TiNTs under visible light illumination for different times. Optic images of bactericidal results from drug-loaded amphiphilic TiNTs with (C) or without D) treatment by visible light irradiation.

visible light is also clearly evident in Figure 5C and D, where a drastic decrease of *E. coli* colonies is observed using the amphiphilic drug release system under visible light irradiation (Figure 5C). These results (Figure 5C,D) demonstrate that the hydrophobic cap can efficiently prevent the leaching of the AMP or the influx of the aqueous surrounding media in dark, that is, the drug delivery system is comparably stable against drug leakage if stored in the dark. XPS data (Figures S3, S9) also confirmed the photocatalytic scission of the hydrophobic and alkyl chains that connect the drug to the wall under visible light irradiation. Moreover, if the gold-decorated top layer is removed before visible light irradiation (Figure S10), the drug molecules cannot be released.

Another very important point evidenced from the results of Figure 5B is that the visible-light-induced photocatalytic effect allows the release of the antibiotic species in a fully functional form. That is, neither the photocatalytic principle nor the direct visible light illumination have a detrimental effect on AMP function, in stark contrast to UV-induced approaches.

In summary, we established a visible-light-controlled platform for drug delivery based on $TiO_2$ nanotubes. The key trigger mechanism is visible light photocatalytic chain scission of an organic monolayer. Activation for visible light is introduced by Au nanoparticles embedded in the hydrophobic cap layer, where Au-SPR with the $TiO_2$ conduction band provides the active species for chain scission. The results, importantly, show that the loaded drug can be photocatalytically released in its fully functional form without photoinduced degradation. We believe the principle shown here, that is, Au SPR/$TiO_2$-induced photocatalytic chain scission by visible light, is not limited to the drug release system demonstrated, but may be expanded to other payload release systems for much wider use.

## Acknowledgements

This work was supported by the National Natural Science Foundation of China (No. 21322504, 11174046, 21275026), the Fundamental Research Funds for the Central Universities (N140505001, N140504006). We also acknowledge financial support from the Alexander von Humboldt Foundation (for Y.Y.S.), ERC, DFG, DFG funCOS, and the DFG cluster of excellence for their financial support.

**Keywords:** antibiotics · drug delivery · nanotubes · surface plasmon resonance

**How to cite:** *Angew. Chem. Int. Ed.* **2016**, *55*, 593–597
*Angew. Chem.* **2016**, *128*, 603–607

[1] a) E. Aznar, M. D. Marcos, R. Martínez-Máñez, F. Sancenón, J. Soto, P. Amorós, C. Guillem, *J. Am. Chem. Soc.* **2009**, *131*, 6833–6843; b) E. M. Bachelder, T. T. Beaudette, K. E. Broaders, J. Dashe, J. M. J. Frechet, *J. Am. Chem. Soc.* **2008**, *130*, 10494–10495; c) S.-M. Lee, H. Chen, C. M. Dettmer, T. V. O'Halloran, S. T. Nguyen, *J. Am. Chem. Soc.* **2007**, *129*, 15096–15097; d) V. C. Anderson, D. H. Thompson, *Biochim. Biophys. Acta Biomembr.* **1992**, *1109*, 33–42.

[2] a) M. L. Viger, W. Sheng, K. Dore, A. H. Alhasan, C. J. Carling, J. Lux, C. G. Lux, M. Grossman, R. Malinow, A. Almutairi, *ACS Nano* **2014**, *8*, 4815–4826; b) S. Y. Park, H. J. Baik, Y. T. Oh, K. T. Oh, Y. S. Youn, E. S. Lee, *Angew. Chem. Int. Ed.* **2011**, *50*, 1644–1647; *Angew. Chem.* **2011**, *123*, 1682–1685.

[3] a) C.-J. Carling, F. Nourmohammadian, J.-C. Boyer, N. R. Branda, *Angew. Chem. Int. Ed.* **2010**, *49*, 3782–3785; *Angew. Chem.* **2010**, *122*, 3870–3873; b) B. P. Timko, T. Dvir, D. S. Kohane, *Adv. Mater.* **2010**, *22*, 4925–4943; c) D. Duracher, F. Sauzedde, A. Elaissari, C. Pichot, L. Nabzar, *Colloid Polym. Sci.* **1998**, *276*, 920–929.

[4] X. Xue, Y. Zhao, L. Dai, X. Zhang, X. Hao, C. Zhang, S. Huo, J. Liu, C. Liu, A. Kumar, W. Q. Chen, G. Zou, X. J. Liang, *Adv. Mater.* **2014**, *26*, 712–717.

[5] A. K. Gaharwar, S. M. Mihaila, A. A. Kulkarni, A. Patel, L. A. Di, R. L. Reis, *J. Controlled Release* **2014**, *187*, 66–73.

[6] a) Z. Liu, J. T. Robinson, X. M. Sun, H. Dai, *J. Am. Chem. Soc.* **2008**, *130*, 10876–10877; b) Z. Liu, X. M. Sun, N. Nakayama-Ratchford, H. Dai, *ACS Nano* **2007**, *1*, 50–56; c) W. Wei, G. H. Ma, G. Hu, D. Yu, T. Mcleish, Z. G. Su, Z. Y. Shen, *J. Am. Chem. Soc.* **2008**, *130*, 15808–15810.

[7] Q. Zhang, M. R. Vakili, X. F. Li, A. Lavasanifar, X. C. Le, *Biomaterials* **2014**, *35*, 7088–7100.

[8] a) A. P. R. Johnston, G. K. Such, F. Caruso, *Angew. Chem. Int. Ed.* **2010**, *49*, 2664–2666; *Angew. Chem.* **2010**, *122*, 2723–2725; b) G. Wu, A. Mikhailovsky, H. A. Khant, C. Fu, W. Chiu, J. A. Zasadzinski, *J. Am. Chem. Soc.* **2008**, *130*, 8175–8177.

[9] N. Murthy, Y. X. Thng, S. Schuck, M. C. Xu, J. M. J. Frechet, *J. Am. Chem. Soc.* **2002**, *124*, 12398–12399.

[10] X. Zhang, L. Meng, Q. Lu, Z. Fei, P. J. Dyson, *Biomaterials* **2009**, *30*, 6041–6047.

[11] L. Meng, X. Zhang, Q. Lu, Z. Fei, P. J. Dyson, *Biomaterials* **2012**, *33*, 1689–1698.

[12] Y. Jiang, G. Liu, X. Wang, J. Hu, G. Zhang, S. Liu, *Macromolecules* **2015**, *48*, 764–774.

[13] Z. Liu, A. C. Fan, K. Rakhra, S. Sherlock, A. Goodwin, X. Chen, Q. Yang, D. W. Felsher, H. Dai, *Angew. Chem. Int. Ed.* **2009**, *48*, 7668–7672; *Angew. Chem.* **2009**, *121*, 7804–7808.

[14] H. Liu, T. J. Webster, *Biomaterials* **2007**, *28*, 354–369.

[15] Y. Y. Song, F. S. Schmidt, S. Bauer, P. Schmuki, *J. Am. Chem. Soc.* **2009**, *131*, 4230–4232.

  

[16] Z. D. Gao, H. F. Liu, C. Y. Li, Y. Y. Song, *Chem. Commun.* **2013**, *49*, 774 – 776.
[17] Z. Zhong, M. Li, D. Xiang, N. Dai, Y. Qing, D. Wang, D. Tang, *Biosens. Bioelectron.* **2009**, *24*, 2246 – 2249.
[18] T. Jayaramudu, G. M. Raghavendra, K. Varaprasad, R. Sadiku, K. M. Raju, *Carbohydr. Polym.* **2013**, *92*, 2193 – 2200.
[19] X. Huang, P. K. Jain, I. H. El-Sayed, M. A. El-Sayed, *Laser. Med. Sci.* **2008**, *23*, 217 – 228.
[20] a) Y. Shi, J. Wang, C. Wang, T. T. Zhai, W. J. Bao, J. J. Xu, X. H. Xia, H. Y. Chen, *J. Am. Chem. Soc.* **2015**, *137*, 7365 – 7370; b) J. B. Priebe, M. Karnahl, H. Junge, M. Beller, D. Hollmann, A. Brückner, *Angew. Chem. Int. Ed.* **2013**, *52*, 11420 – 11424; *Angew. Chem.* **2013**, *125*, 11631 – 11635; c) Y. Tian, T. Tatsuma, *J. Am. Chem. Soc.* **2005**, *127*, 7632 – 7637.
[21] T. Hirakawa, Y. Nosaka, *Langmuir* **2002**, *18*, 3247.
[22] R. L. Fournier, *Basic Transport Phenomena in Biomedical Engineering* **1999**, (Taylor & Francis, Philadelphia).
[23] a) J. Wang, K. Wang, F. B. Wang, X. H. Xia, *Nat. Commun.* **2014**, *5*, 5285; b) J. Wang, H. S. Wang, K. Wang, F. B. Wang, X. H. Xia, *Sci. Rep.* **2014**, *4*, 6723.

Received: September 17, 2015
Revised: November 2, 2015
Published online: November 23, 2015

  